Annals of the Academy of Romanian Scientists
Series on Physics and Chemistry Sciences
ISSN 2559 – 1061 Volume 8, Number 1/2023

ORGANIC LIGHT EMITTING DIODES (OLED)

Silviu POLOȘAN[1]

Abstract. *Organic Light Emitting Diodes (OLED) now reach the third phase concerning efficiency. The first devices are based on pure organic materials, and the second and third generations are based on combinations between metals and organic ligands in so-called organometallics for which their emission external quantum efficiency is increased. The second generation is now widely used in large displays reaching high efficiency because of the spin-orbit coupling between metal and their ligands, which induces intersystem crossing processes. The third generation of OLED comprises an increased external quantum efficiency obtained by adequately choosing the ligands, reaching a theoretical value of 100%. These OLEDs will be briefly described with their advantages and the technologies necessary for next-generation displays.*

Keywords: organic light emitting diodes, organic compounds

DOI https://doi.org/10.56082/annalsarsciphyschem.2023.1.46

1. Introduction

Since 1987, the first electroluminescent device was obtained and the area of organic light emitting diodes (OLED) has grown from the laboratory to the industrial scaling of color displays [1]. The same trend follows the evolution from mono-color, mainly green, to multicolor electroluminescence displays by changing the architecture of the emitting compound embedded in the active layer. The first electroluminescent device was based on the aluminium tris-hydroxyquinoline (Alq_3), and the light emission was due to the delayed fluorescence induced by the presence of Al^{3+} ions. Hence, the exponential current-voltage dependencies accompany the green light of these devices but also exponential luminance versus the applied potential [2,3].

The second generation of OLED devices and color displays, which are now on the market, uses heavy metal ions as the central part of the organometallic compounds such as platinum (Pt), osmium (Os) and the most efficient iridium (Ir) for which the electroluminescence process is based on the phosphorescence as an electronic transition from a forbidden state (triplet state). This process is facilitated by the intersystem crossing from the singlet to triplet transition induced by the spin-orbit coupling between the heavy ion and the organic ligands [4-10]. In these cases, the outer electrons of the metals are involved in the electronic

[1] Dr. Senior Researcher, National Institute of Materials Physics, R-77125 Bucharest, Magurele, Romania, associate member of Romanian Academy (e-mail: silv@infim.ro)

transitions as metal-to-ligand-charge-transfer (MLCT), which significantly increase the lifetime of the light emission [11].

The electroluminescence colors were adjusted to obtain the fundamental red-green-blue (RGB) emissions used in the display panels. The ideal candidate organometallic compound should provide all three colors from three different ligands bounded by the central metallic ion. However, some problems appear for the red emissions because the electronic excitations compete with the non-radiative (thermally assisted) transitions, but also for the blue emissions, where the electronic excitations require higher energies and high electric powers.

Different ligands in several architectures were designed to obtain multicolor emissions. The tris-hydroxyquinoline ligands uses with the Al^{3+} for a delayed fluorescence, and the changing Al^{3+} with Ir^{3+} ions, improves the light emission with an increasing emission lifetime based on phosphorescent processes. Then, the hydroxyquinoline ligands were changed by the most common phenylpiridine bounded by Ir^{3+} ions, creating a more stable green emission based on the MLCT processes towards the ligands. Further, changing one or two ligands to have dual or triple emissions increases exponentially in OLED devices [12, 13]. For example, changing one phenylpiridine ligand with quinoline in the $Ir(ppy)_3$ structure leads to $IrQ(ppy)_2$ organometallic compound with green emission from the MLCT towards pheylpiridine and red emission from the MLCT towards quinoline one [14]. These organometallics exhibit an external quantum efficiency up to 30%. Their stabilities allow the construction of OLED televisions with superior performances compared with the classical LED: fast response, low power consumption, wide view angle, enhanced contrast and thin displays which do not exceed 7 mm with the glass substrate.

The third generation of OLEDs starts with new stable molecules with highly efficient light emissions. It is focused now on technologies like thermally activated delayed fluorescence (TADF), for which the theoretical calculations can achieve 100% efficiency. This novel technology for efficient organic TADF emitter compounds will significantly reduce the cost of OLED production that becomes more environmentally friendly because this new technology will replace the iridium-based organometallics currently employed in the second OLED generation with pure organic or organometallic compounds but with lighter metallic ions and low spin-orbit coupling constant, like selenium [15]. The architecture of these compounds consists of a combination of donor and acceptor radicals on the same molecule, which drastically enhances the charge transport and efficiency compared with the above-described organometallic compounds.

In principle, TADF is obtained by a singlet-singlet excitation, similar to the other compounds, followed by an *intersystem crossing* (ISC) between the singlet

and triplet states and the *reverse intersystem crossing* (RISC) from the triplet back to the singlet state. The emission of light results as singlet-singlet deexcitation. The RISC process is facilitated by two additional conditions: a) energetically reduction between the excited singlet and triplet up to a few tens of electron volts and b) mixing of the states, which facilitate the TADF process.

2. Materials

For the first generation of OLED compounds, the organic molecule tris (8-hydroxyquinoline) aluminium (Alq_3) was synthesized by mixing aluminium hydroxide with 8-hidroxyquinoline at 95 °C. In a typical synthesis, 0.39 g (0.005 mol) of $Al(OH)_3$ was gradually dropped into 80 ml distilled water, which contains 1.45 g (0.01 mol) of 8-hidroxyquinoline. The ratio between 8-hidroxyquinoline and $Al(OH)_3$ was chosen as 2:1, resulting in the most stable meridional Alq_3 compound, in which all the hydroxyquinoline ligands follow the same orientation with meridional symmetry. The reaction time of 6 h led to the production of yellowish Alq_3 powder. In the final stage, the pH was adjusted to the neutral value by dropping NH_3 (precipitating agent) with continuous stirring for the maximum yield. As a result, the synthesized Alq_3 is obtained in the precipitate form [2].

The second generation of organometallics based on Ir^{3+} ions was synthesized with two types of ligands, which required a two-step reaction mechanism. In the first step, iridium chloride hexahydrate reacts with phenylpiridine, forming a $[(C\hat{}N)_2Ir–\mu–Cl]_2$ bridged dimers, further called an intermediate compound. In the second step, the reaction of the intermediate compound with 8-hydroxyquinoline leads to the formation of the final complex, $IrQ(ppy)_2$. The mixture of 2-ethoxyethanol, $[(C\hat{}N)_2Ir–\mu–Cl]_2$, 8-hydroxyquinoline and sodium carbonate was heated to reflux under a nitrogen atmosphere for 24 h [14].

For the TADF compounds, the cross-coupling Suzuki reaction can be performed involving the reaction between an aryl halide and an arylboronic acid to produce a dihalo-phenylpyridine core as the intermediate compound, which reacts with carbazole by an aromatic nucleophilic substitution reaction in the presence of catalysts (NaH or K_2CO_3) with the formation of C-N bonds, in the second step.

3. Device's fabrication

The OLED sandwich structure is based on a glass substrate, an anode indium tin oxide (ITO) deposited on the substrate or a transparent metal with deep Fermi level. The hole transport layer (HTL) usually consisting of PEDOT: PSS polymer, the active layer which is the organometallic compounds dispersed in a transparent and electrically conductive polymer, an electron transport layer (ETL). Finally,

the cathodes in the form of thin films (figure 1 a) or transparent electrospun electrodes (figure 1 b).

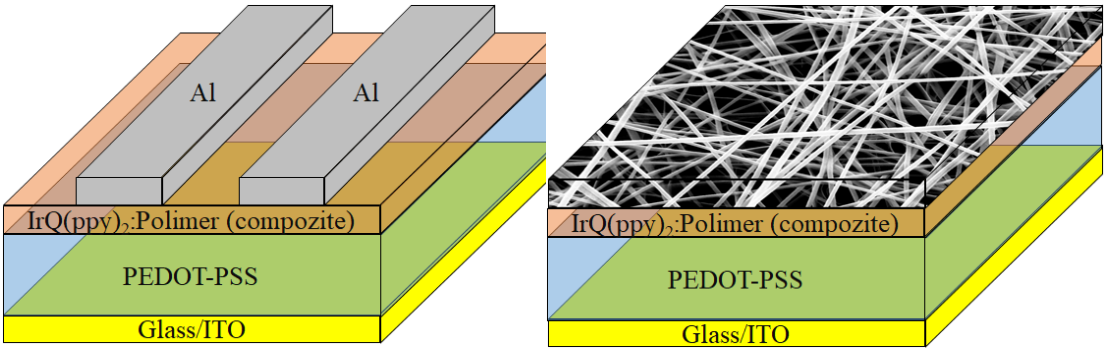

Figure 1. a. Classical OLED with metallic thin film cathodes. **b.** OLED with transparent electrospun cathodes.

The anodes were obtained by magnetron sputtering of ITO or by thermal evaporation for the transparent metals, which can be improved in roughness by low energy electron irradiation for better contacts with the ETL film and better charge injection into the sandwich structure [16]. The HTL, active layer and ETL can be deposited by spin-coating or thermal evaporation, while the metallic cathodes are deposited by thermal evaporation or thermionic vacuum arc [17].

4. Testing methods

The main parameters tested on these OLED sandwich structures are: a) the current density j (A/m^2) from the current-voltage curves; b) the current efficiency as the luminance L in cd/m^2 divided by the current density; c) external quantum efficiency obtained as the ratio between the released number of photons per number of injected electrons. The current-voltage measurements are performed with a source meter such as Keithley 2450, while the luminance, defined as the light electroluminescence under an applied voltage, is measured with a spectroradiometer Konica Minolta CS-2000.

5. Results and discussions

a) The first generation of the OLED based on aluminium tris-hydroxyquinoline compounds was improved by using transparent electrospun cathodes, which enables a double side emission, both through the ITO anode and

the glass substrate, where the metallic cathode is partially transparent in comparison with the neat metallic films (figure 2). The transparent cathode is obtained by the electrospinning procedure of polymethylmethacrylate polymer (PMMA) as web nanowires covered with a metallic layer on both sides and then attached to the OLED sandwich structure by thermal transfer [18].

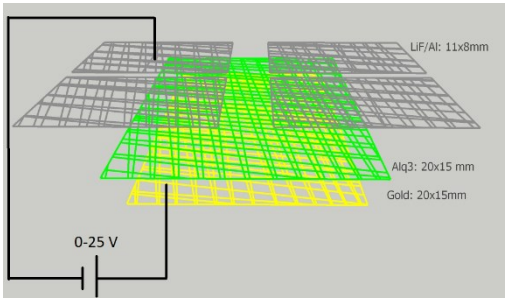

Figure 2. Alq_3-based OLED with transparent electrospun electrodes. Reprinted from ref. [18].

The current-voltage curves differ from the classical neat film cathodes due to a different mechanism of the electron injection into the OLED structures (figure 1a). However, the electron mobility is comparable with the corresponding OLED based on thin films. In addition, the high transparency of the electrodes ranges between 70% and 80%, while the electrical conductivity is similar to other OLED structures based on metal nanofibers.

b)For the second generation of OLED based on the iridium heavy metal ions, the dual emission $IrQ(ppy)_2$ organometallic compound was used in the active layer of a sandwich structure based on glass/ITO/PEDOT: PSS for the anode. The hole transport layer and a transparent cathode ensure a double-side emission, based on PMMA nanowires and gold deposition (figure 1b) [19].

The transmittance of the electroluminescence in the visible range varies from 70% to 80% in the case of PMMA/gold electrode, comparable with glass/ITO electrode. These values follow the electroluminescence properties. After the sputtering deposition, the gold film does not affect the transparency of the web electrode due to the proper optimization of the gold thickness. The higher transparency of the ITO anode will influence the emission properties of the bottom side of the OLED. The presence of the electrospun electrodes enables a double-side emission compared with the single-face emission.

To underline the change point between leakage or diffusion-limited current caused by ohmic contact (low voltage region) and volume-controlled current with

an exponential distribution of traps, known as the opening voltage of diodes, capacitance-voltage measurements have been performed (figure 3 a and b).

In the case of the devices with electrospun cathodes, the inflexion point was measured at 2.5 V (figure 3 a) and is comparable with those with neat film electrodes at around 2 V (figure 3 b). However, for devices with electrospun cathodes, the domain for the applied voltages increases the electroluminescence is restrained between 2.5 V and 10 V, sustaining the non-uniform injection of the electrons in the electrospun devices.

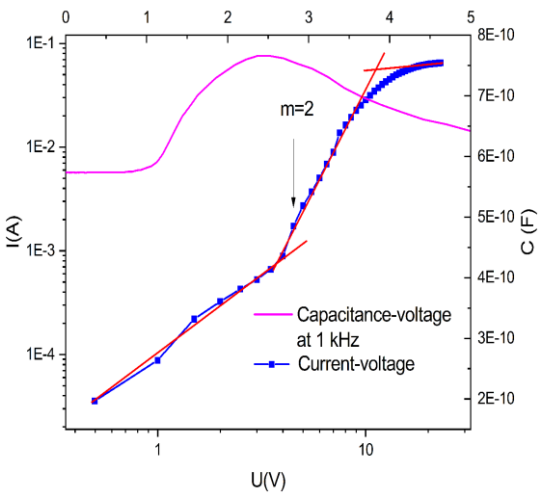

Figure 3 a. Current-voltage dependences and capacitance-voltage for electrospun cathode device. Reprinted from ref. [19].

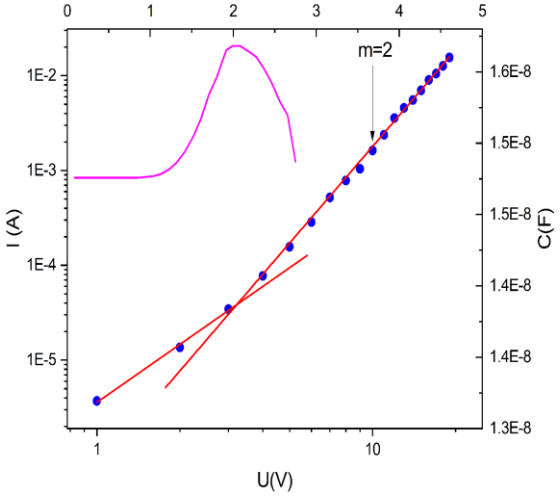

b. Current-voltage dependences and capacitance-voltage measurements for neat cathode films device. Reprinted from ref. [19].

The electroluminescence of the OLED with an electrospun cathode device for a 15 V applied voltage and 55 mA current has three emission peaks centered at 535 nm, 607 nm and 670 nm, with intense red electroluminescence (figure 4 a).

The CIE 1931 color spaces, which describe perceived colors in human color vision, show a stable emission for the applied potential between 9 to 18 V with an orange color having the following coordinates x=0.41 and y=0.39 (figure 4 b).

c) The third generation of OLED devices is based on the TADF mechanism, and the choice of the organic compound used in the active layer depends on the reverse intersystem crossing mechanism. While in the case of organometallic compounds, the valence electrons of the heavy metal ions are subjected to a significant spin-orbit coupling for which the theoretical quantum efficiencies of nearly 100%, the presence of long-living triplet states can cause chemical degradations [20]. Apart from that, spin-orbit (SOC)-based dyes involve relatively rare and expensive heavy elements, which significantly increase their costs.

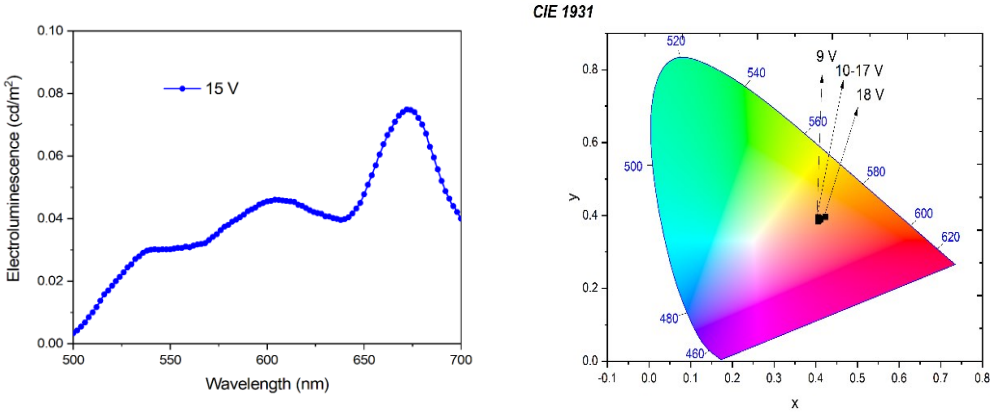

Figure 4. a. Electroluminescence spectral distribution. **b.** CIE 1931 color circle. Reprinted from ref. [19].

In these new OLED generations, the dye molecules in which the last singlet and triplet states are energetically close and vibrationally coupled can exhibit a phenomenon known as thermally activated delayed fluorescence (TADF) [21-25]. The RISC processes can be improved if a small singlet-triplet gap $\Delta E_{ST}=E(S_1) - E(T_1)$ is essential for the following chosen dye molecule. For the ISC process, the spin-orbit interactions can be priory calculated based on the architecture of the dye molecule because the phosphorescence becomes only possible due to the presence of spin-orbit coupling (SOC) effects.

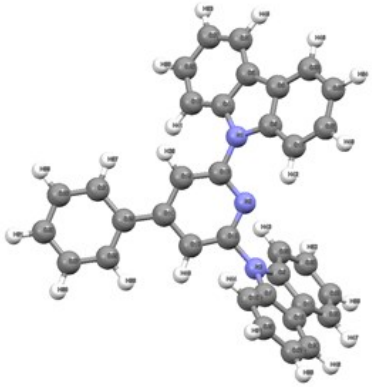

Figure 5. Dye molecule structure.

Density Functional Theory (DFT), especially the Time-Dependent DFT one (TDDFT), becomes computationally viable, especially using the exchange-correlation functionals to model TADF processes. In this context, the spin-orbit coupling effects are treated as perturbations of the systems.

A choice for an organic dye molecule for the TADF is presented in figure 5.

This dye molecule is energetically relaxed using the Spanish Initiative for Electronic Simulations with Thousands of Atoms (SIESTA) DFT software because the spin-orbit calculation is treated as a perturbation process [26]. The relaxed molecule describes the configuration where the minimal energy defines the molecule's stability. Then, a time-dependent (TDDFT) procedure enables the system's geometry to be relaxed in all three relevant electronic states S_0, S_1, and T_1, which are involved in the ISC and RISC processes. For organic structures, the hybrid B3LYP functionals, which stands for Becke, 3-parameter, Lee–Yang–Parr, give better results because incorporate a portion of exact exchange from Hartree–Fock theory with the rest of the exchange–correlation energy from other sources [27]. The exact exchange energy functional is expressed in terms of the Kohn–Sham orbitals rather than the density, termed an implicit density functional. For the spin-orbit coupling, a relativistic scalar zero-order regular approximation (ZORA) to the Dirac equation has been successfully applied to underline the spin–orbit coupling in closed shell molecules [28]. The optimization procedure moves the atoms in such a way to produce a symmetry for a stable structure with minimal energy in several circles of calculation. In ten steps, the electrostatic energy of the system is -17.43108604 Hartree energy units, whereas a Hartree unit is 27.211 eV.

In the ground state (S_0) the molecular charge distribution is mainly focuses on the donor carbazole ligand (figure 6a). In contrast, in the first exited state (S_1), the molecular charge distribution is moved over the acceptor ligand LUMO state (figure 6 b).

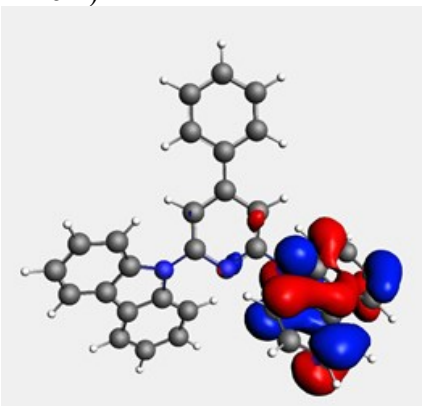

Figure 6 a. The charge distribution in the molecular ground state.

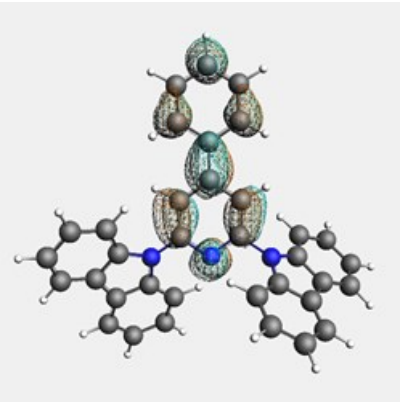

b. The charge distribution in the excited state.

After the charge injection into the LUMO state, the dye molecule returns to the ground state with a charge distribution over the donor ligand accompanied by the electroluminescent process.

From the time-dependent DFT, the first twelve singlets and twelve triples can be determined, which define the spectroscopic properties of the dye molecule. For

example, table 1 gives the first three singlets and three triplets in order of the increasing energy from the S_0 level.

Table 1. The first three singlets and triplets of dye molecule.

No.	*Energy (eV)*	*Symmetry*	*f*
1	2.62384	S_1	0.1593E-01
2	2.56080	T_1	0.000
3	2.86719	S_2	0.7941E-01
4	2.68660	T_2	0.000
5	3.17385	S_3	0.2057E-02
6	2.93336	T_3	0.000

As can be seen, the first singlet state transition is $S_0 \rightarrow S_1$ at an excitation energy of 2.62 eV, while the singlet-triplet gap $\Delta E_{ST}=E(S_1) - E(T_1)$ is 0.063 eV comparable with the thermal energy at room temperature (0.026 eV). It means that the RISC processes can be quickly produced at room temperature, considering the thermal annealing (vibrational processes) and due to the Joule effects given by the charge transport across them. The spin-forbidden transitions appear with vanishing oscillator strengths in a spin-orbit coupling treatment.

The computed absorption spectrum based on the singlet oscillator strengths is presented in figure 7.

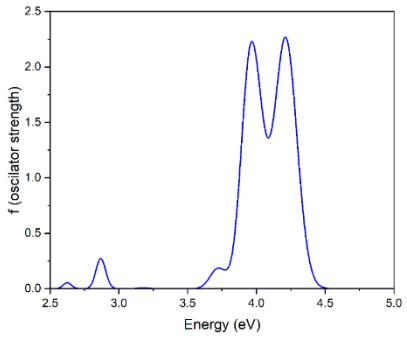

Figure 7. The computed absorption spectrum of dye molecule based on the singlet oscillator strengths.

The absorption spectrum of the dye molecule occurs mainly in the ultraviolet region, but the first singlet states extend the absorption domain toward the green zone around 480 nm.

Without relativistic approaches, the transitions between S_1 and T_1 states are formally forbidden, making the phosphorescence based on intersystem crossing processes impossible. The spin-orbit coupling (SOC) effects, even as scalar approaches, introduces the mixing of the singlet and triplet states, facilitating the ISC process and increasing the phosphorescent transitions as long-lifetime emissions [29].

The rates of intersystem crossing can be calculated based on Fermi's golden rule and provide an expression for the reversed intersystem crossing rate:

$$k_{ISC} = \frac{2\pi}{h} * |V_{SOC}|^2 * \rho_{FCWD} \quad (1)$$

where the $|V_{SOC}|^2$ is understood as the coupling term of the matrix representation of spin-orbit interaction. Considering the T_1 formed from the three sublevels given by the total angular momentum J=−1,0,1, the coupling term is given by:

$$|V_{SOC}|^2 = \frac{1}{3}\sum_{j=-1,0,1} < S_1 |H_{SOC}| T_1^j > * < S_1 |H_{SOC}| T_1^j >^* \quad (2)$$

The ρ_{FCWD} describes the thermokinetic barrier associated with the singlet-triplet transition process and can be computed with the commercial DFT software, such as Amsterdam Density Functional (ADF), based on Marcus Theory (vibrations), Franck-Condon principle and solvation models.

The spin-orbit coupling constant between the first singlet and triplet states $|\langle S_1|H_{SOC}|T_1\rangle|^2$, can be calculated as root mean squares from the sum of squares of spin-orbit coupling matrix elements of all sublevels of the uncoupled states.

The coefficients of the singlet and triplet states for our dye molecule are given in table 2.

Table 2. Spin-orbit coupling matrix elements.

$<S_i\|Hso\|T_j>$	T_1	T_2	T_3
S_1	0.12	1.38	1.00
S_2	1.26	0.19	1.27
S_3	0.37	0.28	0.23

In our case, $|V_{SOC}|^2 = (0.12\ cm^{-1})^2 / 3 = 2.2 \cdot 10^{-10}\ eV^2$ and can be interpreted as the probability for the $S_1 \rightarrow T_1$ transition, which influences the ISC processes and increases the phosphorescent properties of the dye molecule.

6. Conclusions

The preoccupations for the first generation of OLED devices are focused on increasing the light output by using the transparent metallic cathodes or the web fibers metallized electrodes and increasing the charge injection into these structures.

Besides those already described properties, the technologies are focused on a dual and triple electroluminescent emission obtained on the same organometallic compound for the second generation of OLED devices. The second challenge is connected with the increasing external quantum efficiency, mainly given by the internal quantum efficiency of each architectural organometallic molecule and the increasing of the optical coupling between the emissive sandwich layers.

The third generation of OLED is focused on the achievement of 100 % theoretical external quantum efficiency by developing near pure organic donor-acceptor molecules which fulfil the reduction of the energetic gap S_1-T_1 up to the 0.025 eV, which define the thermal activation processes for the RISC mechanisms and the increasing of the spin-orbit coupling coefficients for the singlet-triplet interactions by mixing the pure states and increasing the intersystem crossing mechanism from the S_1 to the T_1 states and therefore the phosphorescence properties of the dye molecules. In this context, changing the sulfur ions with the selenium ions in some TADF molecules increases the spin-orbit coupling due to a larger spin-orbit coupling of the selenium ions compared with those of sulfur.

R E F E R E N C E S

[1] C.W. Tang and S.A. Van Slyke, Appl. Phys. Lett. 51, 913 (1987).
[2] I.C. Radu *et al.,* Opt. Mater. 35(2), 268 (2012).
[3] J.W. Park *et al.,* Int. J. Mol. Sci. 23(11), 5940 (2022).
[4] A.R.G. Smith *et al.,* ChemPhysChem, 12, 2429 2438 (2011).
[5] S.J. Kim *et al.,* Organic Electronics 120 106850 (2023).
[6] D. Tselekidou *et al.,* Materials Science in Semiconductor Processing 163 107546 (2023).
[7] R. Zeng *et al.,* Inorg. Chem. Front., 10, 3263 (2023).
[8] M. Kitahara *et al.,* Organic Electronics 119 106814 (2023).
[9] Z. L. Zhu *et al.,* Mater. Chem. Front., (2023) *Advance Article.*
[10] F. Zhou *et al.,* Eur. J. Inorg.Chem., e202200222 (2022).
[11] M. S. Mehata *et al.,* RSC Adv., 5, 34094 (2015).
[12] S. Polosan *et al.,* J. Phys. Org. Chem., 21(4), 315 (2008).
[13] S. Polosan, *J. Organomet. Chem.* 942, 121814 (2021).

[14] I.C. Ciobotaru *et al.,* J. Lumin. 145, 2592 (2014).
[15] P. Sharif *et al.,* Adv. Func. Mater. 32(47), 2207324 (2022).
[16] S. Polosan *et al.,* IEEE Transactions on Nanotechnology, 21, 823 (2022).
[17] R. Vladoiu *et al.,* J. Alloys & Comp, 869, 159364 (2021).
[18] I.C. Ciobotaru *et al.,* Nanotechnology, 33(39), 395203 (2022).
[19] I.C. Ciobotaru *et al.,* Micromachines, 14(3), 543 (2023).
[20] H. Nakanotani *et al.,* Nature Comm., 5, 4016 (2014).
[21] N. Li *et al.,* Advanced Materials (2023). Advance Article
[22] B. Chen *et al.,* J. Mater. Chem. C, (2023). Advance Article
[23] S. Wu, *et al.,* Angew. Chem.Int. Ed., e202305182 (2023).
[24] J. Liu *et al.,* Chem. Eng. J. 466 142910 (2023).
[25] B. Madushani, *et al.,* Sci Rep 13, 7644 (2023).
[26] https://departments.icmab.es/leem/siesta/
[27] A. D. Becke, J. Chem. Phys. 98 (2): 1372 (1993).
[28] E. Van Lenthe *et al.,* J. Chem. Phys. 105 (15) 6505 (1996).
[29] C.M. Marian, Adv. Rev. 2(2), 187 (2012).

.